EUROPEAN JOURNAL OF MATERIALS SCIENCE AND ENGINEERING
Volume 7, Issue 3, 2022: 169-182 | www.ejmse.ro | ISSN: 2537-4338

EJMSE

DOI: 10.36868/ejmse.2022.07.03.169

FUNCTIONALLY GRADED POROUS MATERIAL FOR PLATES WITH COMPLEX CUT-OUTS AND FINITE ELEMENT MODELING FOR FREE VIBRATION BEHAVIOR

Lan Hoang TON THAT[1,*]

[1]Department of Civil Engineering, HCMC University of Architecture, HCMC, Vietnam

Abstract

The free vibration behaviors of functionally graded porous plates with complex cut-outs are investigated according to a novel C0 type high order shear deformation theory. Both the effect of normal and shear strains are included in this theory as well as shear correction factor is not needed in it. Numerical results have been presented and compared with those available in the literatures. The influences of some parameters like porosity factor and the exponent graded are also studied in this paper. Some new results are finally presented as benchmark for further validation in the future.

Keywords*: functionally graded porous plate; complex cut-out; free vibration; novel C0 type theory; porosity; high order shear deformation theory*.

Introduction

In this era, functionally graded materials with many advantages have been used in various branches of technology. Based on a mixture of ceramic and metal and provided the continuous variation of properties through the thickness of plate, this material has achieved more attention in specific applications, such as nuclear tank, heat exchanger tubes, rocket heat shields, thermoelectric generators, heat-engine components, plasma facings for fusion reactors [1-4], etc. The concept of functionally graded material was first considered in Japan in 1984 during a space plane project, where a combination of materials used would serve the purpose of a thermal barrier capable of withstanding a temperature gradient of 1000 K across a 10 mm section and a surface temperature of 2000 K. The manufacturing process is main reason for the existence of porosities within the materials. Functionally graded porous materials provide desirable properties for some applications as well as the undesirable in others where voids may cause serious problems related to concentrated stresses around them. The change in porosity in multi-directions can lead some drawbacks in the capacity of structures. This material has two types of porosity and then the material modulus are strongly influenced by several parameters. In reality, the prediction of porous materials' properties is not simple because of various reasons, and need to have as much knowledge about it as possible [5-7]. On the other hand, in general cases with complicated geometries or complex conditions, etc., the analytical solutions are also limited.

There are various papers related to the theory of plate structures. For example, author Reddy [8, 9] used a higher-order shear deformation theory (HSDT) to analyse laminated plates for bending, free vibration or buckling behaviors. This theory accounted for parabolic distribution of the transverse shear stresses as well as required no shear correction coefficients. Another simple theory of high-order shear and normal deformation theory was given by Merdaci [10] for

*Corresponding author: tonthathoanglan.247@gmail.com

bending behavior of functionally graded plates with porosity. The stresses at the lower and upper surfaces of the plate are equal zero without using the shear correction factor. Besides, by using Navier's technique, the solution to the problem according to the functionally graded porous plate was solved. A simple integral hyperbolic higher-order shear deformation theory, with undetermined integral terms and only four unknowns, was given by Tahir et al. [11] to formulate a solution for the waves' dispersion relations. The wave propagation's governing equations were derived based on the present integral hyperbolic higher-order shear deformation theory using Hamilton's principle. The eigenvalue problem describing the functionally graded porous plate dispersion relations resting on a viscoelastic foundation was analytically determined. In the paper of Mellal et al. [12], a quasi-3D shear deformation theory was used to predict the wave propagation in functionally graded porous plates resting on Winkler-Pasternak foundation. This theory had a new displacement field that included indeterminate integral terms as well as contains fewer unknown variables taking into account the effect of transverse shear and thickness stretching. In other way, Kumar et al. [13] presented the free vibration response of elastically supported porous bidirectional functionally graded soft-core sandwich rectangular plate with proposed new tangent shape function-based higher-order transverse shear deformation theory. This theory was accomplished to uphold the continuity of transverse shear stresses and zero shear stress conditions on both the extreme surfaces of a plate. By using the Hamilton principle, the governing equations of motion were achieved. These equations were also discretized by the inverse multi-quadric radial basis function-based collocation method and strong form formulation. Their theory and method's accuracy and efficacy were validated and shown that the results of their theory are in close agreement with 3D approach., etc.

It is known that the third-order shear deformation plate theories are the accurate and effective theories due to the modification of the transverse shear components along the thickness of plate and the shear locking free. A novel third-order shear deformation plate theory related to meticulous kinematics of displacements was firstly introduced by the author Shi [14]. The results obtained by the Shi's theory have indicated to be reliable and highly accurate. Beside the analytical approaches, the finite element method is also used in the structural analyses as in [15-17]. For example, based on the MITC3+ shell finite elements, the displacement fields of the higher-order shear deformation theory of Reddy were interpolated by usual linear functions of the three-node triangular element and a cubic supplemented function associated with a node located at the centroid of the element. The transverse shear strain fields were separately approximated to overcome the shear-locking phenomenon. The ES strategy was employed to improve the in-plane strain fields and the in-plane stiffness matrices were calculated by using the line integration on the boundary of the smoothing domains respectively [18]. A few more studies related to functionally graded porous materials are also presented in [19-21]. For instance, to address the interfacial failure problem while maintained the main advantageous features in layered sandwich structures, a novel functionally graded porous plate was given by Chen et al. [21] where the functionally graded porosity offered a smooth stress distribution along the plate thickness so that the remarkable stress mismatch that leaded to interfacial failure in the conventional sandwich structures could be avoided, etc.

Last of all, the free vibration analysis of functionally graded porous plates with complex cut-out using the finite element method and the C^0-type of Shi's theory is firstly presented in this paper as the main concern. The rest sections are established. The brief of functionally graded porous plates, including the two kinds of porosity and the formulation for free vibration analysis are given in Sect.2. The solutions of this study are presented and compared with others from some references in Sect.3. Sect.4 gives out some necessary notes.

Finite element formulation

Consider a functionally graded porous plate with geometrical properties as length *a*, width *b*, and thickness *h*. The coordinate system is depicted in Figure 1. The plate is constructed from a functionally graded material across the thickness direction.

$$V_c = \left(z/h + 0.5\right)^n \text{ and } V_m = 1 - V_c \text{ with } n \geq 0 \tag{1}$$

The porosity volume function α ($0 \leq \alpha \leq 1$) for non-homogeneous material is also described in equations (2-3). In such a way, the material properties related to porosity can be illustrated as:

$$P\left(z,\alpha\right) = \left(P_m - P_c\right)V_m + P_c - \alpha\left(P_m + P_c\right)/2 \quad \text{even porosity} \tag{2}$$

$$P\left(z,\alpha\right) = \left(P_m - P_c\right)V_m + P_c - \alpha\left(P_m + P_c\right)\left(0.5 - \left|z\right|/h\right) \quad \text{uneven porosity} \tag{3}$$

The Shi theory is recalled in this paper for three-dimensional displacement field (u_1, u_2, u_3):

$$u_1\left(x,y,z\right) = u_{01}\left(x,y\right) + \left(\frac{5}{4}z + rz^3\right)\beta_x\left(x,y\right) + \left(\frac{1}{4}z + rz^3\right)u_{03,x}\left(x,y\right) \tag{4}$$

$$u_2\left(x,y,z\right) = u_{02}\left(x,y\right) + \left(\frac{5}{4}z + rz^3\right)\beta_y\left(x,y\right) + \left(\frac{1}{4}z + rz^3\right)u_{03,y}\left(x,y\right) \tag{5}$$

$$u_3\left(x,y,z\right) = u_{03}\left(x,y\right), \qquad r = -\frac{5}{3h^2} \tag{6}$$

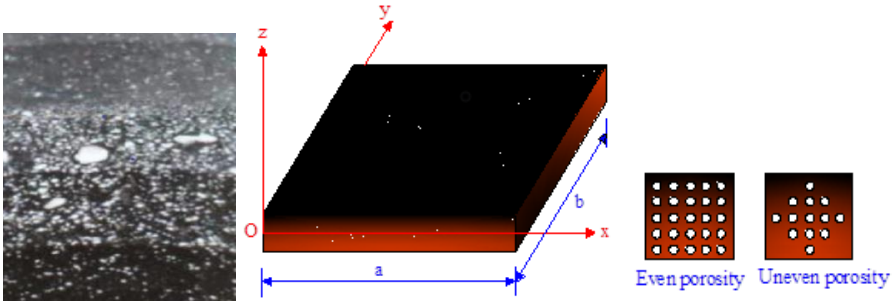

Fig 1. The functionally graded porous plate with both kinds of porosity [22]

This displacement field can be rewritten under C^0-type of HSDT as follows:

$$u_1\left(x,y,z\right) = u_{01}\left(x,y\right) + \left(\frac{1}{4}z + rz^3\right)\beta_x^b\left(x,y\right) + \left(\frac{5}{4}z + rz^3\right)\beta_x^s\left(x,y\right) \tag{7}$$

$$u_2\left(x,y,z\right) = u_{02}\left(x,y\right) + \left(\frac{1}{4}z + rz^3\right)\beta_y^b\left(x,y\right) + \left(\frac{5}{4}z + rz^3\right)\beta_y^s\left(x,y\right) \tag{8}$$

$$u_3(x,y,z) = u_{03}(x,y) \tag{9}$$

Using the small strain assumptions with three axial and transverse displacements (u_{01}, u_{02}, u_{03}), four rotations due to the bending (β_x^b, β_y^b) and shear effects (β_x^s, β_y^s), the strain fields can be shown as follows:

$$\varepsilon_x = u_{01,x} + \frac{1}{4}\left(5\beta_{x,x}^s + \beta_{x,x}^b\right)z + \left(r\beta_{x,x}^s + r\beta_{x,x}^b\right)z^3 \tag{10}$$

$$\varepsilon_y = u_{02,y} + \frac{1}{4}\left(5\beta_{y,y}^s + \beta_{y,y}^b\right)z + \left(r\beta_{y,y}^s + r\beta_{y,y}^b\right)z^3 \tag{11}$$

$$\varepsilon_{xy} = u_{01,y} + u_{02,x} + \frac{1}{4}\left(5\beta_{x,y}^s + \beta_{x,y}^b + 5\beta_{y,x}^s + \beta_{y,x}^b\right)z + r\left(\beta_{x,y}^s + \beta_{x,y}^b + \beta_{y,x}^s + \beta_{y,x}^b\right)z^3 \tag{12}$$

$$\gamma_{yz} = \frac{1}{4}\left(5\beta_y^s + \beta_y^b + 4u_{03,y}\right) + 3r\left(\beta_y^s + \beta_y^b\right)z^2 \tag{13}$$

$$\gamma_{xz} = \frac{1}{4}\left(5\beta_x^s + \beta_x^b + 4u_{03,x}\right) + 3r\left(\beta_x^s + \beta_x^b\right)z^2 \tag{14}$$

In matrix form:

$$\begin{Bmatrix}\boldsymbol{\varepsilon}\\ \boldsymbol{\gamma}\end{Bmatrix} = \begin{Bmatrix}\boldsymbol{\varepsilon}_0\\ \boldsymbol{\gamma}_0\end{Bmatrix} + \begin{Bmatrix}\boldsymbol{\varepsilon}_1\\ 0\end{Bmatrix}z + \begin{Bmatrix}0\\ \boldsymbol{\gamma}_2\end{Bmatrix}z^2 + \begin{Bmatrix}\boldsymbol{\varepsilon}_3\\ 0\end{Bmatrix}z^3 \tag{15}$$

with:

$$\boldsymbol{\varepsilon}_0 = \left[\frac{\partial u_{01}}{\partial x} \quad \frac{\partial u_{02}}{\partial y} \quad \frac{\partial u_{01}}{\partial y} + \frac{\partial u_{02}}{\partial x}\right]^T \tag{16}$$

$$\boldsymbol{\varepsilon}_1 = \frac{1}{4}\left[\left(5\beta_{x,x}^s + \beta_{x,x}^b\right) \quad \left(5\beta_{y,y}^s + \beta_{y,y}^b\right) \quad \left(5\beta_{x,y}^s + 5\beta_{y,x}^s + \beta_{x,y}^b + \beta_{y,x}^b\right)\right]^T \tag{17}$$

$$\boldsymbol{\varepsilon}_3 = r\left[\beta_{x,x}^s + \beta_{x,x}^b \quad \beta_{y,y}^s + \beta_{y,y}^b \quad \beta_{x,y}^s + \beta_{y,x}^s + \beta_{x,y}^b + \beta_{y,x}^b\right]^T \tag{18}$$

$$\boldsymbol{\gamma}_0 = \frac{1}{4}\left[5\beta_y^s + \beta_y^b + 4u_{03,y} \quad 5\beta_x^s + \beta_x^b + 4u_{03,x}\right]^T \tag{19}$$

$$\boldsymbol{\gamma}_2 = 3r\left[\beta_y^s + \beta_y^b \quad \beta_x^s + \beta_x^b\right]^T \tag{20}$$

The constitutive equation is given by:

$$\boldsymbol{\sigma} = \mathbf{D}_1(\mathrm{z})(\boldsymbol{\varepsilon}_0 + \mathrm{z}\boldsymbol{\varepsilon}_1 + \mathrm{z}^3\boldsymbol{\varepsilon}_3) \tag{21}$$

$$\boldsymbol{\tau} = \mathbf{D}_2(z)\left(\boldsymbol{\gamma}_0 + z^2\boldsymbol{\gamma}_2\right) \tag{22}$$

in which:

$$\boldsymbol{\sigma} = \begin{bmatrix} \sigma_x & \sigma_y & \sigma_{xy} \end{bmatrix}^{\mathrm{T}};\ \boldsymbol{\tau} = \begin{bmatrix} \tau_{yz} & \tau_{xz} \end{bmatrix}^{\mathrm{T}} \tag{23}$$

$$\mathbf{D}_1(z) = \frac{E(z)}{1-\nu(z)^2}\begin{bmatrix} 1 & \nu(z) & 0 \\ \nu(z) & 1 & 0 \\ 0 & 0 & (1-\nu(z))/2 \end{bmatrix} \tag{24}$$

$$\mathbf{D}_2(z) = \frac{E(z)}{2(1+\nu(z))}\begin{bmatrix} 1 & 0 \\ 0 & 1 \end{bmatrix} \tag{25}$$

By introducing four-node quadrilateral element with seven degrees of freedom per node, the approximate displacements can be computed as:

$$\mathbf{u}_0 = \mathbf{N}\mathbf{q}_e \tag{26}$$

with

$$\mathbf{u}_0 = \begin{bmatrix} u_{01} & u_{02} & u_{03} & \beta_x^s & \beta_y^s & \beta_x^b & \beta_y^b \end{bmatrix}^{\mathrm{T}} \tag{27}$$

$$\mathbf{N} = \begin{bmatrix} N_1 & N_2 & N_3 & N_4 \end{bmatrix} \tag{28}$$

$$\mathbf{q}_e = \begin{bmatrix} \mathbf{q}_{1e} & \mathbf{q}_{2e} & \mathbf{q}_{3e} & \mathbf{q}_{4e} \end{bmatrix}^{\mathrm{T}} \tag{29}$$

$\mathbf{N}$ and $\mathbf{q}_e$ are the shape function and the unknown displacement vectors. From the equations (15÷29), the strains can be calculated:

$$\boldsymbol{\varepsilon} = \left(\boldsymbol{\Xi}_1 + \boldsymbol{\Xi}_2 + \boldsymbol{\Xi}_3\right)\mathbf{q}_e \tag{30}$$

$$\boldsymbol{\gamma} = \left(\boldsymbol{\Xi}_4 + \boldsymbol{\Xi}_5\right)\mathbf{q}_e \tag{31}$$

in which:

$$\boldsymbol{\Xi}_1 = \sum_{i=1}^{4}\begin{bmatrix} \mathbf{N}_{i,x} & 0 & 0 & 0 & 0 & 0 & 0 \\ 0 & \mathbf{N}_{i,y} & 0 & 0 & 0 & 0 & 0 \\ \mathbf{N}_{i,y} & \mathbf{N}_{i,x} & 0 & 0 & 0 & 0 & 0 \end{bmatrix} \tag{32}$$

$$\mathbf{[\Xi]}_2 = \sum_{i=1}^{4} \begin{bmatrix} 0 & 0 & 0 & \frac{5}{4}\mathbf{N}_{i,x} & 0 & \frac{1}{4}\mathbf{N}_{i,x} & 0 \\ 0 & 0 & 0 & 0 & \frac{5}{4}\mathbf{N}_{i,y} & 0 & \frac{1}{4}\mathbf{N}_{i,y} \\ 0 & 0 & 0 & \frac{5}{4}\mathbf{N}_{i,y} & \frac{5}{4}\mathbf{N}_{i,x} & \frac{1}{4}\mathbf{N}_{i,y} & \frac{1}{4}\mathbf{N}_{i,x} \end{bmatrix} \tag{33}$$

$$\mathbf{[\Xi]}_3 = \sum_{i=1}^{4} \begin{bmatrix} 0 & 0 & 0 & r\mathbf{N}_{i,x} & 0 & r\mathbf{N}_{i,x} & 0 \\ 0 & 0 & 0 & 0 & r\mathbf{N}_{i,y} & 0 & r\mathbf{N}_{i,y} \\ 0 & 0 & 0 & r\mathbf{N}_{i,y} & r\mathbf{N}_{i,x} & r\mathbf{N}_{i,y} & r\mathbf{N}_{i,x} \end{bmatrix} \tag{34}$$

$$\mathbf{[\Xi]}_4 = \sum_{i=1}^{4} \begin{bmatrix} 0 & 0 & \mathbf{N}_{i,y} & 0 & \frac{5}{4}\mathbf{N}_i & 0 & \frac{1}{4}\mathbf{N}_i \\ 0 & 0 & \mathbf{N}_{i,x} & \frac{5}{4}\mathbf{N}_i & 0 & \frac{1}{4}\mathbf{N}_i & 0 \end{bmatrix} \tag{35}$$

$$\mathbf{[\Xi]}_5 = \sum_{i=1}^{4} \begin{bmatrix} 0 & 0 & 0 & 0 & 3r\mathbf{N}_i & 0 & 3r\mathbf{N}_i \\ 0 & 0 & 0 & 3r\mathbf{N}_i & 0 & 3r\mathbf{N}_i & 0 \end{bmatrix} \tag{36}$$

The whole of forces, moments as well as the higher-order of them can be calculated as below:

$$\mathbf{N} = \left\{ \bar{N}_x \;\; \bar{N}_y \;\; \bar{N}_{xy} \right\}^{\mathrm{T}} = \int_{-h/2}^{h/2} \left\{ \sigma_x \;\; \sigma_y \;\; \sigma_{xy} \right\}^{\mathrm{T}} dz = \int_{-h/2}^{h/2} \mathbf{D}_1(z) \left(\boldsymbol{\varepsilon}_0 + z\boldsymbol{\varepsilon}_1 + z^3 \boldsymbol{\varepsilon}_3 \right) dz \tag{37}$$

$$\mathbf{M} = \left\{ \bar{M}_x \;\; \bar{M}_y \;\; \bar{M}_{xy} \right\}^{\mathrm{T}} = \int_{-h/2}^{h/2} \left\{ \sigma_x \;\; \sigma_y \;\; \sigma_{xy} \right\}^{\mathrm{T}} z dz = \int_{-h/2}^{h/2} \mathbf{D}_1(z) \left(\boldsymbol{\varepsilon}_0 + z\boldsymbol{\varepsilon}_1 + z^3 \boldsymbol{\varepsilon}_3 \right) z dz \tag{38}$$

$$\mathbf{P} = \left\{ \bar{P}_x \;\; \bar{P}_y \;\; \bar{P}_{xy} \right\}^{\mathrm{T}} = \int_{-h/2}^{h/2} \left\{ \sigma_x \;\; \sigma_y \;\; \sigma_{xy} \right\}^{\mathrm{T}} z^3 dz = \int_{-h/2}^{h/2} \mathbf{D}_1(z) \left(\boldsymbol{\varepsilon}_0 + z\boldsymbol{\varepsilon}_1 + z^3 \boldsymbol{\varepsilon}_3 \right) z^3 dz \tag{39}$$

$$\mathbf{Q} = \left\{ \bar{Q}_y \;\; \bar{Q}_x \right\}^{\mathrm{T}} = \int_{-h/2}^{h/2} \left\{ \tau_{yz} \;\; \tau_{xz} \right\}^{\mathrm{T}} dz = \int_{-h/2}^{h/2} \mathbf{D}_2(z) \left(\boldsymbol{\gamma}_0 + z^2 \boldsymbol{\gamma}_2 \right) dz \tag{40}$$

$$\mathbf{R} = \left\{ \bar{R}_y \;\; \bar{R}_x \right\}^{\mathrm{T}} = \int_{-h/2}^{h/2} \left\{ \tau_{yz} \;\; \tau_{xz} \right\}^{\mathrm{T}} z^2 dz = \int_{-h/2}^{h/2} \mathbf{D}_2(z) \left(\boldsymbol{\gamma}_0 + z^2 \boldsymbol{\gamma}_2 \right) z^2 dz \tag{41}$$

They are rewritten in the matrix form:

$$\begin{Bmatrix} \mathbf{N} \\ \mathbf{M} \\ \mathbf{P} \\ \mathbf{Q} \\ \mathbf{R} \end{Bmatrix} = \begin{bmatrix} \mathbf{\Psi}_1 & \mathbf{\Psi}_2 & \mathbf{\Psi}_4 & \mathbf{0} & \mathbf{0} \\ \mathbf{\Psi}_2 & \mathbf{\Psi}_3 & \mathbf{\Psi}_5 & \mathbf{0} & \mathbf{0} \\ \mathbf{\Psi}_4 & \mathbf{\Psi}_5 & \mathbf{\Psi}_6 & \mathbf{0} & \mathbf{0} \\ \mathbf{0} & \mathbf{0} & \mathbf{0} & \tilde{\mathbf{\Psi}}_1 & \tilde{\mathbf{\Psi}}_2 \\ \mathbf{0} & \mathbf{0} & \mathbf{0} & \tilde{\mathbf{\Psi}}_2 & \tilde{\mathbf{\Psi}}_3 \end{bmatrix} \begin{Bmatrix} \boldsymbol{\varepsilon}_0 \\ \boldsymbol{\varepsilon}_1 \\ \boldsymbol{\varepsilon}_3 \\ \boldsymbol{\gamma}_0 \\ \boldsymbol{\gamma}_2 \end{Bmatrix} \tag{42}$$

With:

$$\left(\mathbf{\Psi}_1,\ \mathbf{\Psi}_2,\ \mathbf{\Psi}_3,\ \mathbf{\Psi}_4,\ \mathbf{\Psi}_5,\ \mathbf{\Psi}_6\right) = \int_{-h/2}^{h/2} \left(1,\ z,\ z^2,\ z^3,\ z^4,\ z^6\right)\mathbf{D}_1(z)dz \tag{43}$$

$$\left(\tilde{\mathbf{\Psi}}_1,\ \tilde{\mathbf{\Psi}}_2,\ \tilde{\mathbf{\Psi}}_3\right) = \int_{-h/2}^{h/2} \left(1,\ z^2,\ z^4\right)\mathbf{D}_2(z)dz \tag{44}$$

The total strain energy of plate structure due to the whole of forces, moments and the higher-order of them can be given by:

$$U = \frac{1}{2}\int_{V_e} \boldsymbol{\varepsilon}^{\mathrm{T}}\boldsymbol{\sigma}dV - \int_{A_e} \mathbf{u}^{\mathrm{T}}\mathbf{f}dA = \frac{1}{2}\mathbf{q}_e^{\mathrm{T}}\int_{A_e} \begin{pmatrix} \mathbf{\Xi}_1^T\mathbf{\Psi}_1\mathbf{\Xi}_1 + \mathbf{\Xi}_1^T\mathbf{\Psi}_2\mathbf{\Xi}_2 + \mathbf{\Xi}_1^T\mathbf{\Psi}_4\mathbf{\Xi}_3 \\ +\mathbf{\Xi}_2^T\mathbf{\Psi}_2\mathbf{\Xi}_1 + \mathbf{\Xi}_2^T\mathbf{\Psi}_3\mathbf{\Xi}_2 + \mathbf{\Xi}_2^T\mathbf{\Psi}_5\mathbf{\Xi}_3 \\ +\mathbf{\Xi}_3^T\mathbf{\Psi}_4\mathbf{\Xi}_1 + \mathbf{\Xi}_3^T\mathbf{\Psi}_5\mathbf{\Xi}_2 + \mathbf{\Xi}_3^T\mathbf{\Psi}_6\mathbf{\Xi}_3 \\ +\mathbf{\Xi}_4^T\tilde{\mathbf{\Psi}}_1\mathbf{\Xi}_4 + \mathbf{\Xi}_4^T\tilde{\mathbf{\Psi}}_2\mathbf{\Xi}_5 + \mathbf{\Xi}_5^T\tilde{\mathbf{\Psi}}_2\mathbf{\Xi}_4 \\ +\mathbf{\Xi}_5^T\tilde{\mathbf{\Psi}}_3\mathbf{\Xi}_5 \end{pmatrix} dA\mathbf{q}_e - \mathbf{q}_e^{\mathrm{T}}\int_{A_e} \mathbf{N}^{\mathrm{T}}\mathbf{f}dA \tag{45}$$

$$U = \frac{1}{2}\mathbf{q}_e^{\mathrm{T}}\mathbf{K}_e\mathbf{q}_e\ - \mathbf{q}_e^{\mathrm{T}}\mathbf{F}_e = \mathbf{q}_e^{\mathrm{T}}\left(\frac{1}{2}\mathbf{K}_e\mathbf{q}_e\ - \mathbf{F}_e\right) \tag{46}$$

The kinetic energy is shown:

$$T = \frac{1}{2}\int_{V_e} \dot{\mathbf{u}}^{\mathrm{T}}\boldsymbol{\rho}(z)\dot{\mathbf{u}}dV = \frac{1}{2}\dot{\mathbf{q}}_e^{\mathrm{T}}\left\{\int_{V_e} \mathbf{N}^{\mathrm{T}}\mathbf{S}^{\mathrm{T}}\boldsymbol{\rho}(z)\mathbf{S}\mathbf{N}dV\right\}\dot{\mathbf{q}}_e = \frac{1}{2}\dot{\mathbf{q}}_e^{\mathrm{T}}\mathbf{M}_e\dot{\mathbf{q}}_e \tag{47}$$

In which $\mathbf{S}$ is clearly decribed as:

$$\mathbf{S} = \begin{bmatrix} 1 & 0 & \left(\frac{1}{4}\mathrm{z} + r\mathrm{z}^3\right)\frac{\partial}{\partial x} & \left(\frac{5}{4}\mathrm{z} + r\mathrm{z}^3\right) & 0 \\ 0 & 1 & \left(\frac{1}{4}\mathrm{z} + r\mathrm{z}^3\right)\frac{\partial}{\partial y} & 0 & \left(\frac{5}{4}\mathrm{z} + r\mathrm{z}^3\right) \\ 0 & 0 & 1 & 0 & 0 \end{bmatrix} \tag{48}$$

and the matrix $\mathbf{M}_e$ is described here:

$$\mathbf{M}_e = \int_{V_e} \mathbf{N}^{\mathrm{T}}\mathbf{S}^{\mathrm{T}}\boldsymbol{\rho}(z)\mathbf{S}\mathbf{N}dV = \int_{A_e} \mathbf{N}^{\mathrm{T}}\left(\int_{-h/2}^{h/2} \boldsymbol{\rho}(z)\mathbf{S}^{\mathrm{T}}\mathbf{S}dz\right)\mathbf{N}dA \tag{49}$$

The natural frequencies ω can be calculated from:

$$\left(\mathbf{K} - \omega^2\mathbf{M}\right)\mathbf{d} = 0 \tag{50}$$

Verification problems

Now, the verification problems for free vibration behavior of functionally graded porous plates with complex cut-outs are given. Both the simply supported and fully clamped boundary conditions are used in this study. The simply supported (SSSS) boundary condition for this finite element procedure is $u_{02} = u_{03} = \beta_y^s = \beta_y^b = 0$, at $x = 0, a$, $u_{01} = u_{03} = \beta_x^s = \beta_x^b = 0$, at $y = 0, b$ and the fully clamped (CCCC) boundary condition is $u_{01} = u_{02} = u_{03} = \beta_x^s = \beta_x^b = \beta_y^s = \beta_y^b = 0$, at $x = 0, a$ and $y = 0, b$.

Besides, the functionally graded material properties made of the ceramic (Al_2O_3) and the metal (Al) are given as E_c = 380 GPa, ρ_c = 3800 kg/m^3, ν_c = 0.3, E_m = 70 GPa, ρ_m = 2702 kg/m^3, ν_m = 0.3.

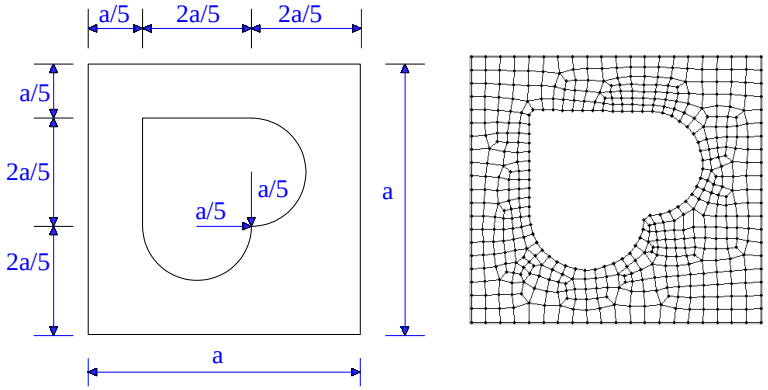

Fig 2. The functionally graded porous plate with complex cut-out I: geometry properties, 425 quadrilateral elements

Firstly, the functionally graded porous plate with complex cut-out I is considered in this section. The geometric properties based on a = 10 m and finite element meshing with 425 quadrilateral elements can be seen in Fig. 2. Both boundary conditions SSSS and CCCC are used in this problem. The frequency of plate is also normalized by formulating $\bar{\omega} = \omega a^2\sqrt{\rho_c / E_c}/h$. Table 1 presents the comparison of the first four normalized frequencies related to this method when porosity factor equals 0 with other methods from other references [23 (*), 24 (**)] using quasi-3D and 3D isogeometric approaches. It can be seen that these proposed values have a good agreement with others from references. Fig. 3 reinforces the above observation respectively.

Table 1. The first four normalized frequencies of SSSS/CCCC functionally graded plate with complex cut-out I and $a/h = 20$

SSSS ($\alpha = 0$, $a/h = 20$)						
Mode	**$n = 0$**			**$n = 0.5$**		
	(*)	**(**)**	**Present**	**(*)**	**(**)**	**Present**
1	7.156	7.160	7.151	6.737	6.750	6.263
2	11.618	11.650	11.556	10.954	11.000	9.998
3	13.107	13.090	13.035	12.355	12.360	11.958
4	20.993	20.990	21.039	19.797	19.840	19.122
CCCC ($\alpha = 0$, $a/h = 20$)						
Mode	$n = 0$			$n = 0.5$		
	(*)	(**)	Present	(*)	(**)	Present
1	15.792	15.850	15.858	14.896	14.980	14.571
2	27.237	27.280	26.632	25.714	25.790	24.818
3	27.351	27.450	27.233	25.821	25.950	25.340
4	33.107	33.220	32.973	31.286	31.440	30.306

Table 2. The SSS/CCCC functionally graded porous plate with complex cut-out I, even porosity, $\alpha = 0.4$, $a/h = 20$ and first six normalized frequencies

($\alpha = 0.4$, $a/h = 20$, Even porosity)						
	CCCC			**SSSS**		
Mode	**$n = 0$**	**$n = 0.5$**	**$n = 1$**	**$n = 0$**	**$n = 0.5$**	**$n = 1$**
1	17.008	13.350	10.142	7.669	6.366	5.533
2	28.561	22.466	17.083	12.393	9.993	8.181
3	29.205	22.984	17.482	13.980	11.226	9.095
4	35.361	27.916	21.301	22.563	18.001	14.328
5	36.517	28.843	22.019	24.208	19.084	14.654
6	44.208	35.010	26.797	34.434	27.272	21.179

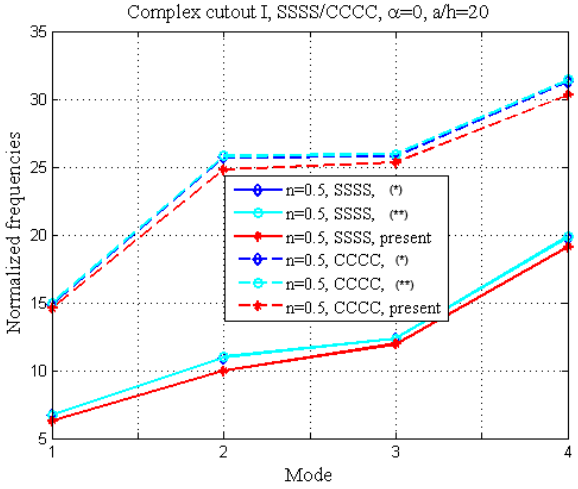

Fig 3. Comparison of the first four normalized frequencies of functionally graded porous plate with $\alpha = 0$, $n = 0.5$ and $a/h = 20$

When porosity factor $\alpha = 0.4$ and length to thickness ratio $a/h = 20$, the first six normalized frequencies of the functionally graded porous plate can be achieved with two kinds of porosity like even and uneven porosity. Tables 2 & 3 give these results under two boundary conditions SSSS and CCCC. We can see that, increase in n from ceramic phase to metal phase reduces the value of natural frequency because of the less stiffness of the plate. Moreover, the highest frequency is obtained for CCCC functionally graded porous plate and the lowest frequency is

given for the SSSS condition due to the restraints of vibration on the boundaries of structure, respectively. Last but not least, the first six mode shapes of functionally graded porous plate with complex cut-out I, a/h = 20, n = 0, α = 0.4, even porosity and CCCC boundary condition are depicted in Fig. 4.

Table 3. The first six normalized frequencies of SSSS/CCCC functionally graded porous plate with complex cut-out I, uneven porosity, α = 0.4 and a/h = 20

(α = 0.4, a/h = 20, Uneven porosity)						
	CCCC			**SSSS**		
Mode	***n* = 0**	***n* = 0.5**	***n* = 1**	***n* = 0**	***n* = 0.5**	***n* = 1**
1	16.775	14.164	12.468	7.590	6.614	6.147
2	28.118	23.767	20.920	12.234	10.483	9.480
3	28.739	24.302	21.377	13.804	11.802	10.635
4	34.746	29.424	25.906	22.262	18.961	16.968
5	35.870	30.383	26.750	23.853	20.181	17.826
6	43.368	36.782	32.401	33.906	28.759	25.491

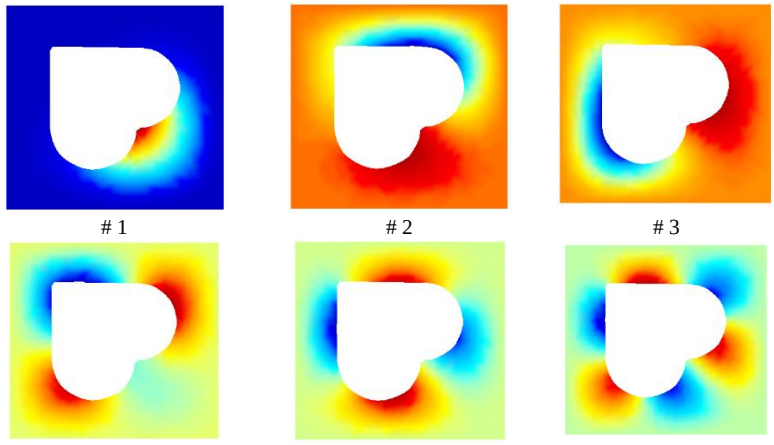

Fig 4. The first six mode shapes of functionally graded porous plate with complex cut-out I, a/h = 20, n = 0, α = 0.4, even porosity and CCCC

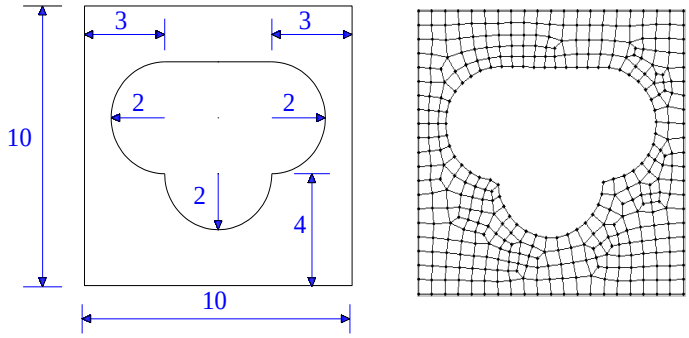

Fig 5. The functionally graded porous plate with complex cut-out II: Geometry properties, 318 quadrilateral elements

Secondly, the functionally graded porous plate with complex cut-out II as Fig. 5 is further reviewed in this paper. Once again, when porosity factor α = 0, length to thickness ratio a/h = 20

and under two kinds of boundary condition, the normalized frequency $\overline{\omega} = \omega a^2 \sqrt{\rho_c / E_c} / h$ of this structure is calculated by using the proposed method. The first four normalized frequencies are shown and compared in Table 4. We can see that these values have a good agreement with others based on quasi-3D isogeometric approach [23 (*)]. Fig. 6 reinforces the above comment respectively. Besides, Tables 5 & 6 also present the first six normalized frequencies of SSSS/CCCC functionally graded porous plate with complex cut-out II, α = 0.4, a/h = 20 and two types of porosity.

Table 4. The first four normalized frequencies of SSSS/CCCC functionally graded plate with complex cut-out II and a/h = 20

SSSS (α = 0, a/h = 20)						
Mode	***n* = 0**		***n* = 0.5**		***n* = 1**	
	(*)	**Present**	**(*)**	**Present**	**(*)**	**Present**
1	7.902	7.861	7.441	7.317	7.269	7.013
2	11.419	11.459	10.770	10.099	10.522	10.004
3	12.822	12.774	12.097	11.976	11.818	11.438
4	21.498	21.508	17.078	16.890	16.767	16.225
CCCC (α = 0, a/h = 20)						
Mode	n = 0		n = 0.5		n = 1	
	(*)	Present	(*)	Present	(*)	Present
1	19.445	19.350	18.352	18.088	17.929	17.391
2	21.980	21.908	20.768	20.137	20.289	19.989
3	29.125	29.132	27.519	27.099	26.883	26.013
4	37.974	37.904	35.930	35.267	35.099	34.876

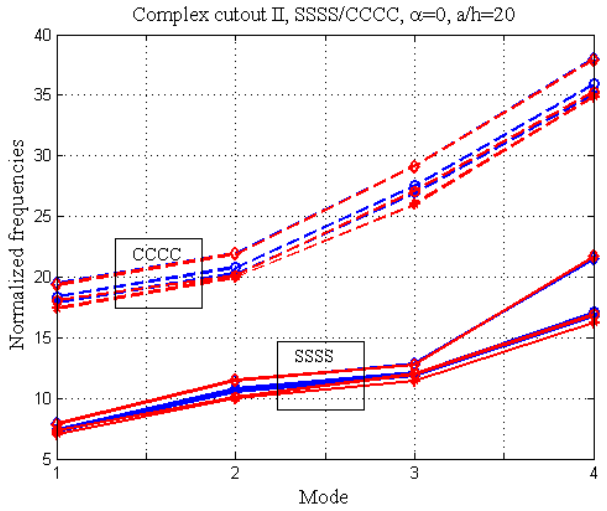

Fig 6. Comparison of the first four normalized frequencies of functionally graded porous plate with α = 0, n = 0, 0.5 & 1 and a/h = 20

Table 5. The first six normalized frequencies of SSSS/CCCC functionally graded porous plate with complex cut-out II, even porosity, α = 0.4 and a/h = 20

(α = 0.4, a/h = 20, Even porosity)						
	CCCC			**SSSS**		
Mode	***n* = 0**	***n* = 0.5**	***n* = 1**	***n* = 0**	***n* = 0.5**	***n* = 1**
1	20.752	16.290	12.370	8.431	7.013	6.135
2	23.495	18.504	14.101	12.289	9.986	8.297
3	31.243	24.598	18.720	13.700	10.990	8.859

(**α = 0.4, a/h = 20, Even porosity**)						
	CCCC			**SSSS**		
Mode	***n* = 0**	***n* = 0.5**	***n* = 1**	***n* = 0**	***n* = 0.5**	***n* = 1**
4	40.650	32.139	24.555	23.066	18.528	15.003
5	42.848	33.903	25.923	28.127	22.133	16.952
6	52.665	41.731	31.928	36.453	29.019	22.820

Table 6. The first six normalized frequencies of SSSS/CCCC functionally graded porous plate with complex cut-out II, uneven porosity, α = 0.4 and a/h = 20

(α = 0.4, a/h = 20, Uneven porosity)						
	CCCC			SSSS		
Mode	n = 0	n = 0.5	n = 1	n = 0	n = 0.5	n = 1
1	20.460	17.276	15.205	8.342	7.278	6.778
2	23.129	19.563	17.225	12.130	10.440	9.502
3	30.743	25.994	22.887	13.522	11.553	10.392
4	39.907	33.817	29.781	22.750	19.451	17.515
5	42.047	35.646	31.396	27.719	23.428	20.677
6	51.614	43.787	38.558	35.866	30.504	27.150

Finally, these six mode shapes are depicted in Fig. 7 as a demonstration of the stability of the proposed element without hourglass phenomenon.

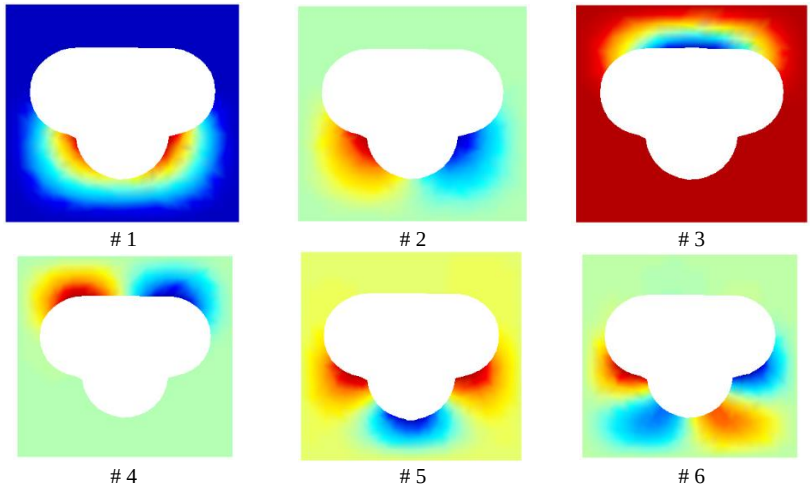

Fig 7. The first six mode shapes of functionally graded porous plate with complex cut-out II, a/h = 20, n = 1, α = 0.4, even porosity and CCCC.

Conclusions

A novel approach for scrutinizing systematically free vibration analysis of functionally graded porous plates with complex cut-outs has been introduced. The C^0-type HSDT which involves seven independent unknowns is provided for the vibration analysis. Both the effect of shear strain and normal deformation are included in the present study and so it does not need any shear correction factor. Functionally graded porous plates with two kinds of porosity are considered and modeled by several meshing. The effectiveness and accuracy of the present approach have been verified by simulating the relevant numerical examples and comparing the results with the available reference solutions.

References

[1] Ichikawa, K., *Functionally Graded Materials in the 21st Century: A Workshop on Trends and Forecasts*. 2001: **Springer US**.

[2] Mahamood, R.M. and E.T. Akinlabi, *Functionally Graded Materials*. 2017: **Springer International Publishing**.

[3] Miyamoto, Y., et al., *Functionally Graded Materials: Design, Processing and Applications*. 1999: **Springer US**.

[4] Shen, H.S., *Functionally graded materials nonlinear analysis of plates and shells*. 2009, **New York, NY, USA: CRC Press Taylor & Francis Group**.

[5] Wang, W., G. Xue, and Z. Teng, *Analysis of Free Vibration Characteristics of Porous FGM Circular Plates in a Temperature Field.* **Journal of Vibration Engineering & Technologies**, 2022.

[6] Wang, Y.Q., Y.H. Wan, and Y.F. Zhang, *Vibrations of longitudinally traveling functionally graded material plates with porosities.* **European Journal of Mechanics - A/Solids**, 2017. **66**: p. 55-68.

[7] Xue, Y., et al., *Free vibration analysis of porous plates with porosity distributions in the thickness and in-plane directions using isogeometric approach.* **International Journal of Mechanical Sciences**, 2019. **152**: p. 346-362.

[8] Reddy, J.N., *Mechanics of laminated composite plates and shells-Theory and analysis*. 2004: **CRC Press**.

[9] Phan, N.D. and J.N. Reddy, *Analysis of laminated composite plates using a higher-order shear deformation theory.* **International Journal for Numerical Methods in Engineering**, 1985. **21**(12): p. 2201-2219.

[10] Merdaci, S. and H. Belghoul, *High-order shear theory for static analysis of functionally graded plates with porosities.* **Comptes Rendus Mécanique**, 2019. **347**(3): p. 207-217.

[11] Tahir, S.I., et al., *An integral four-variable hyperbolic HSDT for the wave propagation investigation of a ceramic-metal FGM plate with various porosity distributions resting on a viscoelastic foundation.* **Waves in Random and Complex Media**, 2021: p. 1-24.

[12] Mellal, F., et al., *Investigation on the effect of porosity on wave propagation in FGM plates resting on elastic foundations via a quasi-3D HSDT.* **Waves in Random and Complex Media**, 2021: p. 1-27.

[13] Kumar, R., et al., *New HSDT for free vibration analysis of elastically supported porous bidirectional functionally graded sandwich plate using collocation method.* Proceedings of the Institution of Mechanical Engineers, **Part C: Journal of Mechanical Engineering Science**, 2022: p. 09544062221090075.

[14] Shi, G., *A new simple third-order shear deformation theory of plates.* **International Journal of Solids and Structures**, 2007. **44**(13): p. 4399-4417.

[15] HL Ton-That, H Nguyen-Van, and T. Chau-Dinh, *Static and buckling analyses of stiffened plate/shell structures using the quadrilateral element SQ4C.* **Comptes Rendus. Mécanique**, 2020. **348**(4): p. 285-305.

[16] Ton-That, H.L., *Plate structural analysis based on a double interpolation element with arbitrary meshing.* **Acta Mechanica et Automatica**, 2021. **15**(2): p. 91-99.

[17] Wu, D., et al., *Dynamic analysis of functionally graded porous structures through finite element analysis.* **Engineering Structures**, 2018. **165**: p. 287-301.

[18] Chau-Dinh, T., et al., *A MITC3+ element improved by edge-based smoothed strains for analyses of laminated composite plates using the higher-order shear deformation theory.* **Acta Mechanica**, 2021. **232**(2): p. 389-422.

[19] Van Vinh, P. and L.Q. Huy, *Finite element analysis of functionally graded sandwich plates with porosity via a new hyperbolic shear deformation theory.* **Defence Technology**, 2022. **18**(3): p. 490-508.

[20] Zenkour, A.M., *Quasi-3D Refined Theory for Functionally Graded Porous Plates: Displacements and Stresses.* **Physical Mesomechanics**, 2020. **23**(1): p. 39-53.

[21] Chen, D., J. Yang, and S. Kitipornchai, *Buckling and bending analyses of a novel functionally graded porous plate using Chebyshev-Ritz method.* **Archives of Civil and Mechanical Engineering**, 2019. **19**(1): p. 157-170.

[22] Rityuj, S.P., Srinivasu G.S., and Sahu, R.K., *Recent advances in the manufacturing processes of functionally graded materials: a review.* **Science and Engineering of Composite Materials**, 2018. **25**(2): p. 309-336

[23] Do, V.N.V. and C.-H. Lee, *Free vibration analysis of FGM plates with complex cut-outs by using quasi-3D isogeometric approach.* **International Journal of Mechanical Sciences**, 2019. **159**: p. 213-233.

[24] Nguyen, K.D. and H. Nguyen-Xuan, *An isogeometric finite element approach for three-dimensional static and dynamic analysis of functionally graded material plate structures.* **Composite Structures**, 2015. **132**: p. 423-439.

Received: June 08, 2022
Accepted: July 22, 2022